Oscillatory fluid flow drives scaling of contraction wave with system size

Jean-Daniel Julien[a] and Karen Alim[a,1]

[a]Biological Physics and Morphogenesis Group, Max Planck Institute for Dynamics and Self-Organization, 37077 Göttingen, Germany

Edited by Herbert Levine, Rice University, Houston, TX, and approved September 9, 2018 (received for review April 6, 2018)

Flows over remarkably long distances are crucial to the functioning of many organisms, across all kingdoms of life. Coordinated flows are fundamental to power deformations, required for migration or development, or to spread resources and signals. A ubiquitous mechanism to generate flows, particularly prominent in animals and amoebas, is actomyosin cortex-driven mechanical deformations that pump the fluid enclosed by the cortex. However, it is unclear how cortex dynamics can self-organize to give rise to coordinated flows across the largely varying scales of biological systems. Here, we develop a mechanochemical model of actomyosin cortex mechanics coupled to a contraction-triggering, soluble chemical. The chemical itself is advected with the flows generated by the cortex-driven deformations of the tubular-shaped cell. The theoretical model predicts a dynamic instability giving rise to stable patterns of cortex contraction waves and oscillatory flows. Surprisingly, simulated patterns extend beyond the intrinsic length scale of the dynamic instability—scaling with system size instead. Patterns appear randomly but can be robustly generated in a growing system or by flow-generating boundary conditions. We identify oscillatory flows as the key for the scaling of contraction waves with system size. Our work shows the importance of active flows in biophysical models of patterning, not only as a regulating input or an emergent output, but also as a full part of a self-organized machinery. Contractions and fluid flows are observed in all kinds of organisms, so this concept is likely to be relevant for a broad class of systems.

active matter | pattern formation | fluid mechanics

Fluid flows are fundamental to the functioning of all organisms. They play an important role in homeostasis, by spreading resources and biochemical signals (1–3). They power deformations driving migration of many motile cells (4–6) and can even directly impact organism size (7). Surprisingly, even in the absence of a pacemaker like a heart, flows are coordinated on vastly different scales ranging from the size of a single migrating cell of about 20 μm (8, 9), via the *Caenorhabditis elegans* gonad of about 450 μm (10, 11), to the *Drosophila* embryos of about 500 μm (12), to acellular slime molds of more than 2 cm in size (13). The physical mechanism of how coordinated flows can self-organize particularly in a single cellular envelope remains unknown.

Animal and slime mold cells are lined with an actomyosin cortex situated just below their cellular envelope, enclosing the cells' fluid cytoplasm. This actomyosin meshwork forms an active viscoelastic material (14, 15). It contracts under myosin motor activity and thereby drives the enclosed cytoplasm to flow into a less contracted part of the cell (1, 16). Long-range flows adapting to system size therefore require a spatial organization of cortex contractility. The mechanism driving the coordination of cortex contraction across a cell or an organism is unclear.

Already in the early 1980s Oster and Odell (17, 18) explored the idea that a contraction-triggering chemical, like calcium, could explain dynamic, oscillatory patterns of actomyosin activity in the cell cortex. However, the dynamic patterns' spatial component was not investigated. Calcium is necessary to generate actomyosin contractions in many biological systems (19–22). Additionally, calcium is regulated by mechanical stretching, via mechanosensitive channels (23–26). Consequently, cortex expansion triggers the influx of calcium which in turn leads to contraction. Due to the widespread importance of cortex activity in developmental processes, this feedback is of general interest, investigated in mechanochemical models (27). Models describing the cortex as a fluid (28) or as a poroelastic medium (29), where active stress is up-regulated by a chemical immersed in this medium, account for short-range traveling waves of contractions and oscillatory flows. However, the mechanistic insight is missing that can account for coordination of contractions on scales beyond the intrinsic length scale of the dynamic system and thus account for very long-range fluid flows scaling with system size.

Particularly, the slime mold *Physarum polycephalum* is renowned for long-range coordination of cortex contractions. Here, fluid flows scale with organism size from 2 mm to at least 2 cm (13). Again, flows are known to power organism migration (6, 30). Moreover, stimulants that alter cortex contractility have recently been found to be advected with the fluid flows inside the cell (2). This observation suggests that the physical transport by fluid flows is the key to long-range spatial coordination of cortex contractions and fluid flows.

Here, we investigate in a tubular geometry the self-organization of cortex contractions, coupled to a contraction-triggering chemical which is advected with the flows of the fluid cytoplasm. The simple two-component model is unstable toward self-sustained cortex oscillations as cortex stretching triggers the increase of the contraction-triggering chemical concentration. A linear analysis of the model predicts traveling-wave solutions of

Significance

Long-range fluid flows are crucial for the functioning of many organisms, as they provide forcing for migration and development and spread resources and signals. How flows can span vastly different scales is unclear. Here, we develop a minimal, two-component model, coupling the mechanics of a cell's cortex to a contraction-triggering chemical. The chemical itself is spread with the fluid flows that arise due to the cortex contractions. Through theoretical and numerical analysis, we find that the oscillatory component of the flows can give rise to robust scaling of contraction waves with system size—much beyond predicted length scales. This mechanism is likely to work in a broad class of systems.

Author contributions: J.-D.J. and K.A. designed research, performed research, and wrote the paper.

The authors declare no conflict of interest.

This article is a PNAS Direct Submission.

[1]To whom correspondence should be addressed. Email: karen.alim@ds.mpg.de.

This article contains supporting information online at www.pnas.org/lookup/suppl/doi:10.1073/pnas.1805981115/-/DCSupplemental.

Published online October 3, 2018.

cortex shape and the intrinsic wavelength of the dynamic instability is derived. In contrast to our analytic prediction, numerical solutions of the model in a tube with periodic boundaries show a probabilistic distribution of five different patterns of traveling waves. Although the tube is twice as long as the expected intrinsic wavelength, in one of these patterns the traveling wave scales with tube length. Further analysis shows that scaling can be robustly generated in growing tubes with periodic boundary conditions or by flow-generating boundary conditions in nongrowing tubes. We identify oscillatory flows as the key to the scaling of contraction waves with system size. The ubiquity of fluid flows in biological and nonliving systems suggests that this nontrivial scaling could be broadly relevant in active matter.

Results

Coupling of Tubular-Shaped Cortex with Contraction-Triggering Chemical. A cell showing coordinated cytoplasmic fluid flows in general has a distinctive viscous fluid phase separated from a surrounding viscoelastic actomyosin cortex. The nature of long-range flows typically entails a tubular cell shape. We here consider as a minimal model an active, viscoelastic tube of length L, filled with a fluid. Tube shape is fully defined by the tube's radius $a\,(z,t)$ along the tube's axial position z and over time t. The tube's temporal evolution directly follows from the conservation of the fluid volume within the tube,

$$\frac{\partial a^2}{\partial t} = -\frac{\partial}{\partial z}\left(a^2 \bar{u}\right), \qquad [1]$$

where $\bar{u}(z,t)$ denotes the cross-sectionally averaged fluid flow velocity along the tube. Fluid flow is powered by contractions of the tube and thus by the stress $\sigma(z,t) = \sigma_c + \sigma_e$ acting radially within the tube's cross-section (Fig. 1). We distinguish σ_c, the contractile stress stemming from actomyosin activity within the cortex, and σ_e, the counteracting viscoelastic restoring stress of the cell. For long slender tubes, $a/L \ll 1$, lubrication approximation applies. The Stokes equation for the fluid velocity simplifies to

$$\bar{u} = -\frac{a^2}{8\mu}\frac{\partial}{\partial z}\left(\sigma_c + \sigma_e\right), \qquad [2]$$

where μ denotes the dynamic viscosity of the fluid. We approximate the cell's material properties to be dominated by a linear viscoelastic response following a Kelvin–Voigt model with a small nonlinearity to suppress potential divergences. Abbreviating radial deformation as $\epsilon = [a - a^*]/a^*$ with respect to the constant equilibrium radius a^*, the restoring stress is given by

$$\sigma_e = E\epsilon + \kappa\epsilon^3 + \eta\frac{\partial \epsilon}{\partial t}, \qquad [3]$$

where E and η denote the tube's effective elastic modulus and viscosity, respectively, and κ is the strength of the nonlinear response. Note that E and η incorporate both the elastic properties and the thickness of the cell cortex.

In light of the role of calcium in coordinating actomyosin activity, we describe the strength of the cortex contractile stress to be proportional to the concentration of a contraction-triggering chemical c. In addition, contractions may self-amplify as more actin fibers overlap in a contracted cortex following observations for low myosin concentrations typical for nonmuscle cells (31, 32). Inversely, overlap decreases in an expanded cortex, reducing potential contractility. Consequently, the contractile stress is represented by

$$\sigma_c = \sigma_0 \frac{\mathcal{C}}{\mathcal{C}^*}\left(1 - \frac{\epsilon}{\epsilon_\sigma}\right). \qquad [4]$$

Here, $\mathcal{C} = \pi a^2 c$ represents the chemical concentration integrated across the cross-section of the cell, $\mathcal{C}^*$ is the equilibrium concentration, σ_0 describes the active tension at equilibrium, and ϵ_σ is the typical deformation for the change in fiber overlap to become significant for contractility. The chemical itself constantly cycles between an inactive state and an active state in the cytoplasm with release rate p_c and capture rate d_c. We assume the amount of inactive chemical to be abundant and therefore not limiting the dynamics here. Importantly, motivated by our knowledge of calcium regulation by mechanical deformations (23–26), additional chemical is released at the cell's membrane upon cortex stretch with ϵ_c denoting the corresponding typical deformation scale. Now, we further incorporate spatial coupling as we account for the advection and diffusion of the contraction-triggering chemical. Reflecting the tubular cell shape we assume the chemical to average out quickly across the tube's cross-section by diffusion, with diffusivity D, compared with the advective transport with velocity $\bar{u}$ along the tube of length L, $a^2\bar{u}/DL \ll 1$. This assumption

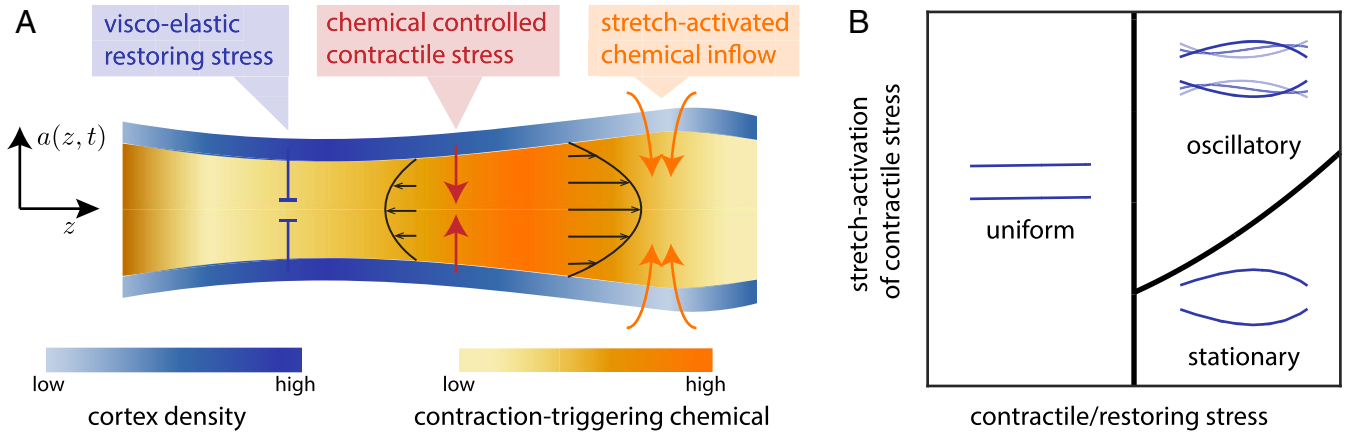

Fig. 1. Illustration of the model predicting self-sustained contraction waves. (*A*) A tubular-shaped cell lined with an actomyosin cortex (blue) enclosing the liquid cytoplasm carrying a contraction-triggering chemical (orange). Chemically controlled contractile cortex stress is balanced by viscoelastic restoring stress. Small cortex contractions self-amplify as more actin overlaps in a contracted cortex, shown in variations in cortex density. Cortex stretch leads to inflow of contraction-triggering chemical, allowing for self-sustained oscillations. Contractions are coupled spatially as the chemical is advected with the cytoplasmic flows (parabolic lines) resulting from cortex deformations. (*B*) Phase diagram depicting a region of uniform, stationary pattern and oscillatory patterns.

warrants the use of Taylor dispersion for a tube of varying radius (33),

$$\frac{\partial \mathcal{C}}{\partial t} = 2\pi a \left[p_c \left(1 + \frac{\epsilon}{\epsilon_c}\right) - d_c \frac{\mathcal{C}}{\pi a^2} \right] + \frac{\partial}{\partial z} \left[-\mathcal{C}\bar{u} + \left(D + \frac{a^2 \bar{u}^2}{48D} \right) \pi a^2 \frac{\partial}{\partial z} \left(\frac{\mathcal{C}}{\pi a^2} \right) \right]. \quad [5]$$

Here, the $2\pi a$ factor in the kinetics term stems from chemical release at the surface of the tube. Note, that chemical release in the bulk, i.e., a factor of πa^2 instead, does not alter the model's dynamics described below (*SI Appendix, Linear Stability Analysis*).

Stretch-Activated Chemical Inflow Controls Self-Sustained Oscillations. At zero fluid flow the tube's radius is uniformly at its rest value of $a = a^*$. Similarly, the chemical concentration is at a constant value of $C^* = \pi a^{*2} p_c / d_c$ throughout the tube. This uniform state is unstable with respect to small perturbations as a small deformation of the tube radius grows when the contractile stress of scale σ_0/ϵ_σ exceeds restoring stress (Fig. 1*B*). Thus, the relative stretch parameterized by ϵ_σ drives the short wave instability of the system. A stretched cortex additionally ignites the inflow of the contraction-triggering chemical. Chemical inflow results in contractions, thus decreasing the deformation and initiating the oscillation. Consistent with this intuitive reasoning, linear stability analysis shows that the uniform state is unstable if σ_0/ϵ_σ is large enough compared with the tube's elastic modulus E, diffusion D, and capture rate d_c, all factors limiting the development of fluctuations,

$$\frac{\sqrt{\frac{\sigma_0}{\epsilon_\sigma} - E}}{\sqrt{\frac{16\mu D}{a^{*2}}} + \sqrt{\frac{2d_c\eta}{a^*}}} > 1 \quad [6]$$

(*SI Appendix, Instability Condition*). The wavelength of the most unstable mode is given by

$$\lambda_{\text{lin}} = \pi a^* \sqrt{\frac{\eta}{\mu}} \left(\sqrt{\frac{a^{*2}\left(\frac{\sigma_0}{\epsilon_\sigma} - E\right)}{D\mu}} - 4 \right)^{-\frac{1}{2}}. \quad [7]$$

The scale of coordinated flows set by this intrinsic wavelength here arises from the competition between diffusion D and viscosity η, increasing the wavelength by filtering out perturbations on a short scale, and contractility, amplifying the fluctuations locally and controlled essentially by σ_0/ϵ_σ. Approximating $\mu D \ll \frac{\sigma_0 a^{*2}}{\epsilon_\sigma} - E a^{*2}$, the linear analysis also gives a constraint for an oscillatory instability

$$\sqrt{\frac{2\sigma_0}{\epsilon_c} \frac{a^*}{\eta d_c}} > 1 + \left(\frac{\sqrt{\frac{\sigma_0}{\epsilon_\sigma} - E}}{\sqrt{\frac{16\mu D}{a^{*2}}} + \sqrt{\frac{2d_c\eta}{a^*}}} \right)^2 \quad [8]$$

(Fig. 1*B*). The oscillation frequency ω can be derived (*SI Appendix*, Eq. **S1**). The result confirms the intuitive idea that oscillations occur if the stretch-activated chemical release, controlled by $1/\epsilon_c$, is strong enough to counterbalance the self-amplifying deformation of the tube. Based on these analytical results we expect the system to generate spontaneous contractile waves of a wave size given by the most unstable mode λ_{lin}.

Multiple Patterns of Contractions Arise in a Periodic Tube. To study the self-organization of contractile waves in organisms of varying sizes, we numerically solve model Eqs. **1** and **5** in tubes of different lengths L and measure the sizes of the contractile wave patterns λ (Fig. 2). As model parameters, we choose physiological values for calcium kinetics and actomyosin cortex mechanics

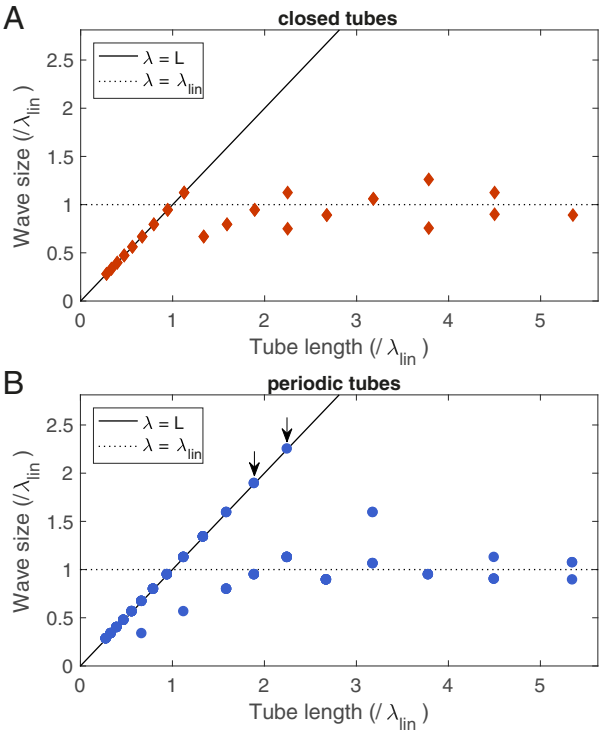

Fig. 2. Contraction wave can scale with tube length. (*A* and *B*) Size of self-sustained contraction waves λ for tubes of different lengths L, for closed (*A*) and periodic (*B*) boundary conditions. Linear stability analysis predicts wave size to be bound by the intrinsic wavelength of the most unstable mode λ_{lin} (dotted line) as observed numerically for a closed tube. However, wave size can scale with tube length (arrows in *B*) for periodic boundary conditions. Each data point denotes an individual simulation.

(*Materials and Methods*). Tube radius is chosen to match *P. polycephalum*—most renowned for scaling contraction waves. The model is further verified by comparing the numerically observed phase relationship between fluid flow and contraction-triggering chemical to experimental data of *P. polycephalum* (34). The model predicts the nontrivial change of phase relationship along the tube (*SI Appendix*, Fig. S3), robust against changes in model parameters. Among ambiguous observations on the role of calcium in *P. polycephalum* (35, 36), complemented by theoretical models (37), this experimental verification of our model promotes that calcium activates actin–myosin contractions in *P. polycephalum* as is common in living organisms.

To determine the size of the waves, we computed the power spectral density of the radius $a(z,t)$ averaged over 10 oscillation periods and identified the dominant mode. As "wave size" λ we denote the inverse of the dominant mode. Note that wave size is not always equivalent to wavelength, in particular if the patterns are antisymmetric (see Fig. 3 *B* and *E*, for examples of patterns with different wavelength and equal wave size). Simulations with closed boundary conditions (Fig. 2*A*) fully match our expectations from linear stability analysis, namely waves increasing with tube length up to an upper bound given by the intrinsic wavelength corresponding to the most unstable mode λ_{lin}. Surprisingly, in simulations with periodic boundary conditions (Fig. 2*B*) we observe waves exceeding λ_{lin}, scaling with tube length instead.

Characterizing more precisely the variety of wave patterns, we screen multiple runs with different initial perturbations, for the intermediate tube length $L = 2\lambda_{\text{lin}}$, with periodic boundary conditions (Fig. 3 and *SI Appendix*, Fig. S2). Observed wave patterns can be divided into five cases, by wave size and

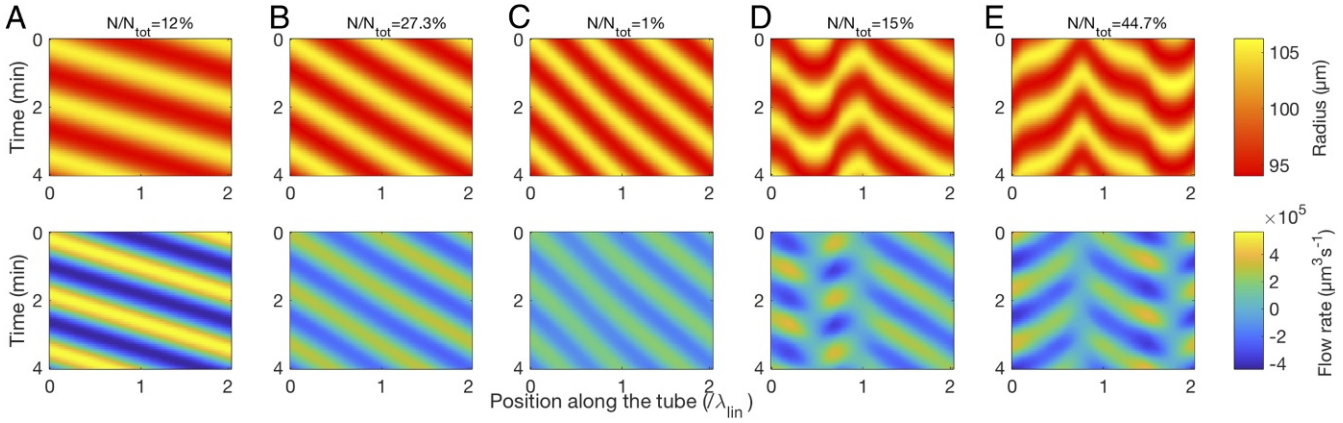

Fig. 3. Stable wave patterns in a periodic tube twice as large as the intrinsic wavelength $L = 2\lambda_{\text{lin}}$. (*A*–*E*) Tube radius (*Top*) and resulting fluid flow rate (*Bottom*) along a tube (horizontal axis) and time (vertical axis). Probability of each pattern in 300 independent runs is denoted above the radius plots.

period-averaged flow rate along the tube (see *SI Appendix*, Fig. S6 for details on the identification of the patterns). There are one, two, or three waves traveling in the same direction (Fig. 3*A*, *B*, or *C*, respectively), two antisymmetric waves (Fig. 3*E*), or two asymmetric waves (Fig. 3*D*). The single wave matching tube length (Fig. 3*A*) generates the strongest net fluid flow, exceeding unidirectional multiple wave patterns (Fig. 3 *B* and *C*) and asymmetric waves (Fig. 3*D*). Patterns with antisymmetric waves (Fig. 3*E*) do not create a net flow due to their invariance under space flipping, thus not providing any mass transport or long-range mixing. Patterns occur with very different probabilities with only 12% showing the most efficient pattern regarding mixing and transport, where the wave scales with tube length. In general, net flow and maximum flow increase with wave size (38) (*SI Appendix*, Fig. S5), and thus generating waves scaling with system size is fundamental for organisms whose size varies vastly. What measures can make this most efficient pattern more robust? What mechanism drives the scaling of the contractions with the size of the tube?

Growth of the Tube Leads to the Robust Scaling of the Wave. To investigate robustness and the mechanism behind the scaling of contractile waves we performed simulations of growing tubes and measured wave size for periodic or closed boundaries (Fig. 4). Tubes grow linearly, starting from $0.2\lambda_{\text{lin}}$ in length.

In agreement with linear stability analysis we find that waves in tubes with closed boundaries grow with tube length only up to the upper bound λ_{lin}. However, for periodic boundary conditions, waves scale with the length of the tube up to sevenfold λ_{lin} (Fig. 4). From linear stability analysis the wavelength $\lambda = 7\lambda_{\text{lin}}$ is an unstable but not oscillating state (*SI Appendix*, Fig. S1), suggesting another mechanism beyond linear stability analysis at play. Above this limit to the scaling L_{lim}, the wave splits into six or seven smaller waves matching roughly λ_{lin} (Fig. 4). Note that while the wave size scales with system size, the period of contractions barely changes (*SI Appendix*, Fig. S5), in accordance with observations (39). Results are robust against variations in parameters. Particularly, changing the fluid viscosity μ varies the scaling limit L_{lim} and the factor of mode multiplication $n = L_{\text{lim}}/\lambda_{\text{lin}}$. Contrary to previous reaction–diffusion systems capable of mode doubling or tripling when simulated on growing domains (40), many values of n are accessible; see *SI Appendix*, Fig. S7 for $n \in [5, 8]$. From Eq. **7**, we can see that the predicted wavelength scales like $\lambda_{\text{lin}} \propto \mu^{-1/4}$. On the other hand, a dimensional analysis of the advective term in Eq. **5** leads to a typical scale proportional to $\mu^{-1/2}$, consistent with our simulations showing $L_{\text{lim}} \propto \mu^{-0.51}$ (*SI Appendix*, Fig. S7). As λ_{lin} and L_{lim} scale differently with viscosity, the mode-multiplication factor n changes accordingly. Noteworthy, decreasing the viscosity increased the scaling limit. A lower viscosity does not change any mechanical properties of the tube but increases the flow velocity and thus advection of the contraction-triggering chemical. This suggests that flow-driven transport is crucial for the observed scaling mechanism and the upper scaling limit.

Scaling of the Wave Is Due to Oscillatory Flows. To distinguish the role of net flow J_{net} and oscillatory flow J_{osc} in establishing the scaling, we investigated dynamics in tubes with an imposed inflow of $J = J_{\text{net}} + J_{\text{osc}}\cos(\omega t)$ on one end of the tube. To limit our study to a 2D parameter space, we set ω to the natural angular frequency of our system (*SI Appendix*, Eq. **S1**). The values of J_{net} and J_{osc} were chosen to be comparable with the values generated spontaneously in simulations of periodic tubes (*SI Appendix*, Fig. S8).

Imposed flow boundary conditions result in long-range contraction patterns (Fig. 5). Interestingly, J_{net} and J_{osc} have different effects on the observed wave size. Contrary to our expectations, the net flow J_{net} has little impact on contraction wave size. The oscillatory part of the flow J_{osc}, on the other hand, increases sharply the wavelength for any value of J_{net}.

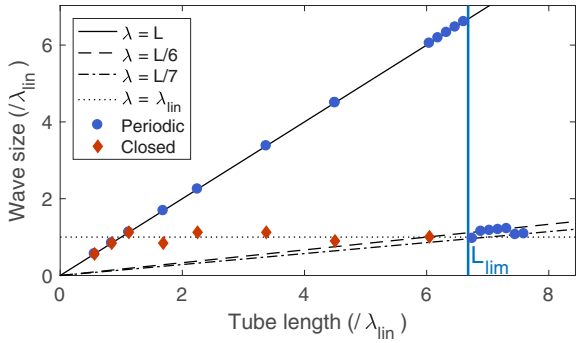

Fig. 4. Scaling of the contraction wave in growing, periodic tubes. Shown is wave size λ for tubes with periodic (blue circles) and closed (red diamonds) boundaries, grown to different lengths L. While wave size in closed tubes saturates at λ_{lin} (dotted line) as predicted from linear stability analysis, waves in tubes with periodic boundaries scale robustly with tube length up to sevenfold the predicted length (blue vertical line). Each data point represents an independent run of a tube grown from an initial $L = 0.2\lambda_{\text{lin}}$.

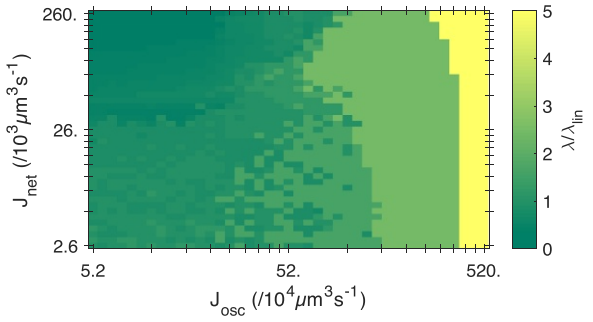

Fig. 5. Scaling of wave with system size governed by an oscillatory flow component at the tube boundary. Shown is a heat map of wave sizes in tubes of $L = 5\lambda_{\text{lin}}$ with an imposed flow $J = J_{\text{net}} + J_{\text{osc}} \cos(\omega t)$ at one boundary. Full scaling arises at high oscillatory flow J_{osc} almost independent of net flow J_{net}.

Interestingly, the time necessary to establish a stable pattern of contractions is shorter as the wave size grows (*SI Appendix*, Fig. S8). Thus, we find that oscillating flow at the boundary, rather than net flow, is the key to scaling with system size much beyond the intrinsic length scale of the instability.

Discussion

We have studied the self-organization of long-range fluid flows in tubular-shaped cells, due to the coupling of cortex contractions to an advected, contraction-triggering chemical. Our minimal two-component model system describing cortex and chemical dynamics predicts self-sustained contraction waves of wave size λ_{lin}. Numerical simulations of the model confirm these predictions in tubes with closed boundaries. However, in tubes with periodic boundary conditions we find flows to scale with tube length much beyond the predicted wave size λ_{lin}. Robust scaling is observed when tubes are grown longer than λ_{lin}, "mode multiplying" at a scaling limit $L_{\text{lim}} = n\lambda_{\text{lin}}$, $n = 6.6$. Simulations of fluids with different viscosities and tubes with imposed inflow show that the oscillatory flow is the key to this unexpected scaling on such long length scales.

From a dynamical systems point of view, previous work accounted for scaling contraction waves only when also the period of contraction scaled (41), whereas in our mechanism the period barely changes. Also the observation of mode multiplying at factors of up to 8 vastly exceeds previous observations of mode doubling or mode tripling (40). Within our model we find that mode multiplying is determined by the ratio between the scaling limit L_{lim} and the linearly unstable wavelength λ_{lin}. The impact of the viscosity of the cytoplasm, as an example, was investigated, and the different scaling with viscosity, $\lambda_{\text{lin}} \propto \mu^{-1/4}$ and $L_{\text{lim}} \propto \mu^{-1/2}$, explained the splitting of the contraction wave to different modes.

The oscillatory nature of fluid flows allowed by periodic boundary conditions or by imposed flow is crucial to generate scaling beyond the intrinsic wavelength λ_{lin} (Eq. **7**). The value of the intrinsic wavelength may vary broadly between different systems. Assuming our representative parameter values, that contractility is of the same order as stiffness $\frac{\sigma_0}{\epsilon_\sigma} - E \sim E$, and taking into account only that cell elastic modulus and cortex viscosity scale with cortex thickness h over cell radius a^*, a rule of thumb for the intrinsic wavelength is $\lambda_{\text{lin}} \simeq 1\, m^{\frac{1}{2}} (h a^*)^{\frac{1}{4}}$. This rule of thumb implies that only based on the intrinsic wavelength, a doubling in system size would requires a 16-fold increase in radius to allow the intrinsic wavelength to match the doubled system size. Alternatively, oscillatory flow boundary conditions are required to allow for scaling with system size beyond the intrinsic wavelength as the system grows. Given the possible range of biological parameters, this rule of thumb sets a scale for the radius over which long-range scaling due to oscillatory flows is likely to be at work. Note that the scale predicted here is only a rough estimate as our mechanochemical model accounts for only the role of calcium and additional cortex regulation machinery might be important in a specific system (5). Moreover, measurements of the mechanical and geometrical properties of the cell cortex show large variations and increase further the uncertainty. The key insight is that oscillatory fluid flows can generate scaling contraction waves and that it may be worth checking for their role in large systems, exceeding the intrinsic wavelength.

For the system best studied for its cortex-driven cytoplasmic flows, *P. polycephalum*, and with parameter values inferred from related organisms where necessary (*Materials and Methods*), the predicted wave size is $\lambda_{\text{lin}} = 7.1\,\text{mm}$, about an order of magnitude smaller than the coordinated contraction waves observed on scales of up 2 cm (13), but well within the range of $L_{\text{lim}} = 4.7\,\text{cm}$, in agreement with our predictions. At these large scales *P. polycephalum* forms a network of tubes with more viscous bags pooling fluid at the growing fronts. It is fascinating to speculate how the network morphology impacts the dynamics of contractile waves. It is likely that the contractions of the viscous bags at the growing fronts here do serve as pumps very much similar to the imposed flow boundary conditions we implemented. The growing fronts could thereby also account for the resurrection of scaling contraction waves after contraction stopped due to harmful external stimuli (42). In contrast to *P. polycephalum* to date detailed quantitative data are lacking in other systems to allow for quantitative comparison. However, cortex contractions and oscillatory flows are very general components for many other systems, even beyond the single cell. Thus, the interplay of fluid flows and mechanical oscillations resulting in scaling might be broadly relevant.

In general, our model broadens the budding understanding of the fundamental role of cytoplasmic flows in a large class of biophysical systems (1, 43–45). In very diverse systems, flows appear to be a fundamental part of a self-organized machinery. In our case, their oscillations are crucial to drive and organize patterns of contractions on a large scale, a mechanism likely present in many other biological systems. More fundamentally, our result opens perspectives on how including active advection in classical reaction–diffusion frameworks leads to unexpected observations such as scaling.

Materials and Methods

Implementation. Numerical solutions of the model equations were explored with a custom-written Crank–Nicholson scheme implemented in MATLAB (The Mathworks). Simulations started from the spatially uniform equilibrium value for tube radius and chemical concentration. To perturb the stable state, uncorrelated, Gaussian fluctuations of SD 0.01 were added to the radius. Three kinds of boundary conditions were implemented: periodic, closed, or flow. For flow boundary conditions, the radius and the chemical concentration at the boundaries of the tube are both assumed to be equal to their value at the uniform equilibrium, and fluid flow is imposed on one end of the tube. In growing tubes, linear growth is simulated by changing dynamically the mesh size used for spatial discretization. The mesh is refined when the length of the tube doubled. The growth rate is small compared with the contraction period to decouple the dynamics of the system from growth. When tubes reach their target lengths, simulations are continued for roughly 200 additional contraction periods to ensure that growth has no impact on the simulated pattern.

Parameters. Simulations parameters were $\mu = 1.5 \times 10^{-3}$ Pa·s for the viscosity of the cytoplasm (46), $a^* = 100\,\mu\text{m}$ for the radius of the viscoelastic tube, $E = 10$ Pa for its effective stiffness [assuming a Young's modulus of 100 Pa (47, 48) and a thickness of the tubes of $h = a^*/10$], $\eta = E \times 24s$ for its effective viscosity (47, 49, 50), $\kappa = 100E$ for the nonlinear elasticity, $\sigma_0 = 3E$ for the active stress (48, 51), $D = 3.33 \times 10^{-10}\,\text{m}^2\cdot\text{s}^{-1}$ (37, 52) for the diffusion of the tension activator in the cytoplasm, $a^*c^*/(2p_c) = a^*/(2d_c) = 96$ s

(23, 24) for the timescale of its regulation, $\epsilon_c = 0.3$ for the threshold of its stretch-activated supply, and $\epsilon_\sigma = 2$ for the stretch inhibition of the active stress. The mechanical parameters, particularly κ and ϵ_σ, were chosen to result in deformations of about 10%, typical for *P. polycephalum* (13). The resulting flow velocities in our simulations were around $\bar{u} = 10\ \mu\text{m}\cdot\text{s}^{-1}$ to $30\ \mu\text{m}\cdot\text{s}^{-1}$, matching cytoplasmic flows for *P. polycephalum* (2).

ACKNOWLEDGMENTS. This work was supported by the Max Planck Society.

1. Goldstein RE, van de Meent JW (2015) A physical perspective on cytoplasmic streaming. *Interface Focus* 5:20150030.
2. Alim K, Andrew N, Pringle A, Brenner MP (2017) Mechanism of signal propagation in *Physarum polycephalum*. *Proc Natl Acad Sci USA* 114:5136–5141.
3. Koslover EF, Chan CK, Theriot JA (2017) Cytoplasmic flow and mixing due to deformation of motile cells. *Biophys J* 113:2077–2087.
4. Allen RD, Allen NS (1978) Cytoplasmic streaming in amoeboid movement. *Annu Rev Biophys Bioeng* 7:469–495.
5. Blaser H, et al. (2006) Migration of zebrafish primordial germ cells: A role for myosin contraction and cytoplasmic flow. *Dev Cell* 11:613–627.
6. Rieu JP, Delanoe-Ayari H, Takagi S, Tanaka Y, Nakagaki T (2015) Periodic traction in migrating large amoeba of Physarum polycephalum. *J R Soc Interface* 12:20150099.
7. Tominaga M, et al. (2013) Cytoplasmic streaming velocity as a plant size determinant. *Dev Cell* 27:345–352.
8. Yoshida K, Soldati T (2006) Dissection of amoeboid movement into two mechanically distinct modes. *J Cell Sci* 119:3833–3844.
9. Lämmermann T, et al. (2008) Rapid leukocyte migration by integrin-independent flowing and squeezing. *Nature* 453:51–55.
10. Wolke U, Jezuit EA, Priess JR (2007) Actin-dependent cytoplasmic streaming in C. elegans oogenesis. *Development* 134:2227–2236.
11. Atwell K, et al. (2015) Mechano-logical model of *C. elegans* germ line suggests feedback on the cell cycle. *Development* 142:3902–3911.
12. Hecht I, Rappel WJ, Levine H (2009) Determining the scale of the Bicoid morphogen gradient. *Proc Natl Acad Sci USA* 106:1710–1715.
13. Alim K, Amselem G, Peaudecerf F, Brenner MP, Pringle A (2013) Random network peristalsis in *Physarum polycephalum* organizes fluid flows across an individual. *Proc Natl Acad Sci USA* 110:13306–13311.
14. Kruse K, Joanny JF, Jülicher F, Prost J, Sekimoto K (2005) Generic theory of active polar gels: A paradigm for cytoskeletal dynamics. *Eur Phys J E* 16:5–16.
15. Prost J, Jülicher F, Joanny JF (2015) Active gel physics. *Nat Phys* 11:111–117.
16. Taylor DL, Condeelis JS, Moore PL, Allen RD (1973) The contractile basis of amoeboid movement: I. The chemical control of motility in isolated cytoplasm. *J Cell Biol* 59:378–394.
17. Oster GF, Odell GM (1984) Mechanics of cytogels I: Oscillations in Physarum. *Cell Motil* 4:469–503.
18. Oster GF, Odell GM (1984) A mechanochemical model for plasmodial oscillations in Physarum. *Modelling of Patterns in Space and Time*, eds. Jäger W, Murray JD (Springer, Berlin), Vol 55, pp 302–317.
19. Smith DA, Saldana R (1992) Model of the Ca2+ oscillator for shuttle streaming in Physarum polycephalum. *Biophys J* 61:368–380.
20. Schuster S, Marhl M, Höfer T (2002) Modelling of simple and complex calcium oscillations. From single-cell responses to intercellular signalling. *Eur J Biochem* 269:1333–1355.
21. Levasseur M, Carroll M, Jones KT, McDougall A (2007) A novel mechanism controls the Ca2+ oscillations triggered by activation of ascidian eggs and has an absolute requirement for Cdk1 activity. *J Cell Sci* 120:1763–1771.
22. Antunes M, Pereira T, Cordeiro JV, Almeida L, Jacinto A (2013) Coordinated waves of actomyosin flow and apical cell constriction immediately after wounding. *J Cell Biol* 202:365–379.
23. Glogauer M, et al. (1997) Calcium ions and tyrosine phosphorylation interact coordinately with actin to regulate cytoprotective responses to stretching. *J Cell Sci* 110:11–21.
24. Lee J, Ishihara A, Oxford G, Johnson B, Jacobson K (1999) Regulation of cell movement is mediated by stretch-activated calcium channels. *Nature* 400:382–386.
25. Matthews BD, Overby DR, Mannix R, Ingber DE (2006) Cellular adaptation to mechanical stress: Role of integrins, Rho, cytoskeletal tension and mechanosensitive ion channels. *J Cell Sci* 119:508–518.
26. Vogel V, Sheetz M (2006) Local force and geometry sensing regulate cell functions. *Nat Rev Mol Cell Biol* 7:265–275.
27. Veksler A, Gov NS (2009) Calcium-actin waves and oscillations of cellular membranes. *Biophys J* 97:1558–1568.
28. Bois JS, Jülicher F, Grill SW (2011) Pattern formation in active fluids. *Phys Rev Lett* 106:028103.
29. Radszuweit M, Alonso S, Engel H, Bär M (2013) Intracellular mechanochemical waves in an active poroelastic model. *Phys Rev Lett* 110:138102.
30. Lewis OL, Zhang S, Guy RD, del Alamo JC (2015) Coordination of contractility, adhesion and flow in migrating Physarum amoebae. *J R Soc Interface* 12:20141359.
31. Hanson J, Lowy J (1963) The structure of F-actin and of actin filaments isolated from muscle. *J Mol Biol* 6:46–60.
32. Janson LW (1991) Modulation of contraction by gelation/solation in a reconstituted motile model. *J Cell Biol* 114:1005–1015.
33. Mercer GN, Roberts AJ (1994) A complete model of shear dispersion in pipes. *Japan J Indust Appl Math* 11:499–521.
34. Zhang S, Guy RD, Lasheras JC, del Álamo JC (2017) Self-organized mechano-chemical dynamics in amoeboid locomotion of *Physarum* fragments. *J Phys D Appl Phys* 50:204004.
35. Kuroda R, Hatano S, Hiramoto Y, Kuroda H (1988) Change of cytosolic Ca-ion concentration in the contraction and relaxation cycle of Physarum microplasmodia. *Cell Dynamics*, ed Tazawa M (Springer, Vienna) Vol 1, pp 72–80.
36. Yoshiyama S, Ishigami M, Nakamura A, Kohama K (2009) Calcium wave for cytoplasmic streaming of Physarum polycephalum. *Cell Biol Int* 34:35–40.
37. Radszuweit M, Engel H, Bär M (2014) An active poroelastic model for mechanochemical patterns in protoplasmic droplets of Physarum polycephalum. *PLoS One* 9: e99220.
38. Shapiro AH, Jaffrin MY, Weinberg SL (1969) Peristaltic pumping with long wavelengths at low Reynolds number. *J Fluid Mech* 37:799–825.
39. Kuroda S, Takagi S, Nakagaki T, Ueda T (2015) Allometry in Physarum plasmodium during free locomotion: Size versus shape, speed and rhythm. *J Exp Biol* 218:3729–3738.
40. Crampin EJ, Gaffney EA, Maini PK (2002) Mode-doubling and tripling in reaction-diffusion patterns on growing domains: A piecewise linear model. *J Math Biol* 44:107–128.
41. Kessler DA, Levine H (2016) Nonlinear self-adapting wave patterns. *New J Phys* 18:122001.
42. Bäuerle FK, Kramar M, Alim K (2017) Spatial mapping reveals multi-step pattern of wound healing in Physarum polycephalum. *J Phys D Appl Phys* 50:434005.
43. Woodhouse FG, Goldstein RE (2013) Cytoplasmic streaming in plant cells emerges naturally by microfilament self-organization. *Proc Natl Acad Sci USA* 110:14132–14137.
44. Monteith CE, et al. (2016) A mechanism for cytoplasmic streaming: Kinesin-driven alignment of microtubules and fast fluid flows. *Biophys J* 110:2053–2065.
45. Quinlan ME (2016) Cytoplasmic streaming in the Drosophila oocyte. *Annu Rev Cell Dev Biol* 32:173–195.
46. Puchkov EO (2013) Intracellular viscosity: Methods of measurement and role in metabolism. *Biochem (Mosc) Suppl Ser A Membr Cell Biol* 7:270–279.
47. Naib-Majani W, Teplov VA, Baranowski Z (1988) Morphology and visco-elastic properties of Physarum strands during the steady-state of their contractile behavior. *Cell Dynamics*, Protoplasma, ed Tazawa M (Springer, Vienna), Vol 1, pp 57–63.
48. Salbreux G, Charras G, Paluch E (2012) Actin cortex mechanics and cellular morphogenesis. *Trends Cell Biol* 22:536–545.
49. Feneberg W, Westphal M, Sackmann E (2001) Dictyostelium cells' cytoplasm as an active viscoplastic body. *Eur Biophys J* 30:284–294.
50. Saha A, et al. (2016) Determining physical properties of the cell cortex. *Biophys J* 110:1421–1429.
51. Maître JL, Niwayama R, Turlier H, Nédélec F, Hiiragi T (2015) Pulsatile cell-autonomous contractility drives compaction in the mouse embryo. *Nat Cell Biol* 17:849–855.
52. Donahue BS, Abercrombie RF (1987) Free diffusion coefficient of ionic calcium in cytoplasm. *Cell Calcium* 8:437–448.